Effect of Sr substitution for Ca on the $Ca_3Co_4O_9$ thermoelectric properties

G. Constantinescu[1], Sh. Rasekh[1], M. A. Torres[2], J. C. Diez[1], M. A. Madre[1], A. Sotelo[1]

[1]ICMA (UZ-CSIC), Dpto. de Ciencia y Tecnología de Materiales y Fluidos, C/María de Luna 3, E-50018, Zaragoza (Spain)

[2]Universidad de Zaragoza, Dpto. de Ingeniería de Diseño y Fabricación, C/María de Luna 3, E-50018, Zaragoza (Spain)

Abstract

$Ca_{3-x}Sr_xCo_4O_9$ polycrystalline thermoelectric ceramics with small amounts of Sr have been synthesized by the classical solid state method. Microstructural characterizations have shown that all the Sr has been incorporated into the $Ca_3Co_4O_9$ and $Ca_3Co_2O_6$ structures and no Sr-based secondary phases have been produced. Apparent density measurements have shown that samples slightly increase their density until 0.05 Sr content, decreasing for higher contents. Electrical resistivity decreases and Seebeck coefficient slightly raises when Sr content increases until 0.07 Sr addition. The improvement in both parameters leads to higher power factor values than the usually obtained in samples prepared by the conventional solid state routes and close to those obtained in textured materials.

Keywords: Doping; Sintering; Cobaltites; Electrical properties; Thermopower.

Corresponding author: A. Sotelo

e-mail: asotelo@unizar.es

Address: Dept. Ciencia de Materiales; C/Mª de Luna, 3; 50018-Zaragoza; Spain

Tel: +34 976762617

Fax: +34 976761957

1. Introduction

Thermoelectric (TE) materials can transform a temperature gradient to electrical power directly due to the well-known Seebeck effect. The conversion efficiency of such materials is usually quantified by the dimensionless figure of merit ZT, $TS^2/\rho\kappa$ (in which the electrical part S^2/ρ is also called power factor, PF), where S is the Seebeck coefficient (or thermopower), ρ the electrical resistivity, κ the thermal conductivity, and T is the absolute temperature [1]. This important characteristic has focused attention on this type of materials in order to be applied as waste heat recovery devices [2] or solar thermoelectric generators [3]. Furthermore, they can also be used as heating/refrigeration devices [4]. Taken into account the above expression, high performance thermoelectric materials should possess large Seebeck coefficient and low electrical resistivity and thermal conductivity. Low electrical resistivity is necessary to minimize Joule heating, while a low thermal conductivity helps to maintain a large temperature gradient between the hot and cold sides in the thermoelectric device.

Nowadays TE devices based on intermetallic materials, such as Bi_2Te_3 or $CoSb_3$, with high ZT values, are industrially used at relatively low temperatures, e.g. in vehicles exhaust. However, they cannot be applied in devices working at high temperatures under air due to their degradation or heavy metals evaporation. These temperature limitations were overcome by the discovery in 1997 of attractive thermoelectrical properties in $Na_2Co_2O_4$ ceramics [5]. From the discovery of this thermoelectric oxide, much work has been performed on different cobaltite ceramic families as promising thermoelectric materials for high temperature applications, as the Bi-M-Co-O-based (M: alcaline earth)

materials [6-8]. Nowadays, research is focused on Bi-free ceramic materials with high thermoelectric performances and higher thermal stability, such as $Ca_3Co_4O_9$, with interesting thermoelectric properties [9,10].

Crystallographic studies performed on those Co-based materials have demonstrated that they posses a monoclinic structure which is, in turn, composed of two different layers. These layers show an alternate stacking of a common conductive CdI_2-type hexagonal CoO_2 layer with a two-dimensional triangular lattice and a block layer composed of insulating rock-salt-type (RS) layers. The two sublattices (RS block and CdI_2-type CoO_2 layer) possess common a- and c-axis lattice parameters and β angles, but different b-axis length, causing a misfit along the b-direction [11,12]. Furthermore, it has also been found that the Seebeck coefficient values are governed by the incommensurability ratio and/or the charge of the RS block layer between the CoO_2 ones [13]. This is the basis for the modification of thermoelectric properties of a given material via chemical substitutions, as Sb^{3+} for Ca^{2+} in $Ca_3Co_4O_9$ [14], or Pb^{2+} for Bi^{3+} in $Bi_2Sr_2Co_{1.8}O_x$ or $Bi_2Ca_2Co_{1.7}O_x$ [15-17]. Other improvements can be produced by metallic Ag additions where an increase on the materials performances is produced by raising the electrical connectivity between the grains [18,19].

On the other hand, the high crystallographic anisotropy of these materials leads to the formation of plate-like grains during the sintering process. This shape anisotropy opens the route to align preferentially the grains using physical, mechanical and/or chemical processes. Such processes should allow the alignment of the conducting planes leading to macroscopic properties comparable to those obtained on single crystals. Numerous methods have been

reported to be efficient in producing well aligned bulk materials, in these or in similar anisotropic systems, such as hot uniaxial pressing [20,21], spark plasma sintering [22,23], microwave texturing [24], laser floating zone melting (LFZ) [25,26], electrically asisted laser floating zone (EALFZ) [27,28], templated grain growth (TGG) [29], *etc*. The main advantage of these techniques is the production of materials with very low electrical resistivity values due to the preferential alignment of conducting planes with the current flow direction. On the other hand, they possess some drawbacks, as the high price of the spark plasma device and the relatively long processing time of the hot uniaxial pressing or the TGG. In the case of the processes involving samples melting, it has been reported that the electrical properties are strongly dependent on the growth speed [24,30-32].

The aim of this work is to study the effect of small amounts of Sr for Ca substitution on the microstructure and high temperature thermoelectric properties of $Ca_{3-x}Sr_xCo_4O_y$ prepared by the classical solid state synthetic route. The structural and microstructural modifications produced by the Sr incorporation in the crystal structure will be related with the changes on the thermoelectric performances.

2. Experimental

$Ca_{3-x}Sr_xCo_4O_9$ polycrystalline ceramic materials, with x = 0.00, 0.01, 0.03, 0.05, 0.07, and 0.10, were prepared by the conventional solid state route using $CaCO_3$ (Panreac, 98 + %), $SrCO_3$ (Panreac, 98 + %), and Co_2O_3 (Aldrich, 98 + %) commercial powders as starting materials. They were weighed in the appropriate proportions, well mixed and ball milled for 30 minutes at 300 rpm, in

acetone media, in an agate ball mill. The obtained slurry has been heated under infrared radiation until all the acetone has been evaporated. The dry mixture was then manually milled in order to avoid the presence of agglomerates in the next steps. After milling, the homogeneous mixture was thermally treated twice at 750 and 800ºC for 12h under air, with an intermediate manual milling in order to assure the total decomposition of carbonates, as reported previously [10], which improve the mixture reactivity in the sintering processes. After the thermal treatments, the powders were uniaxially pressed at 400 MPa for 1 minute in order to obtain green ceramic parallelepipeds (3 mm x 2.5 mm x 14 mm), with an adequate size for their thermoelectric characterization. The green ceramics were subsequently sintered in the optimal conditions found in previous works, and consisting in one step heating at 900 ºC for 24 h with a final furnace cooling [10].

Powder X-ray diffraction (XRD) patterns have been systematically recorded in order to identify the different phases in the thermoelectric sintered materials. Data have been collected at room temperature, with 2θ ranging between 5 and 60 degrees, using a Rigaku D/max-B X-ray powder diffractometer working with Cu Kα radiation. Apparent density measurements have been performed on several samples for each composition after sintering, using 4.677 g/cm^3 as theoretical density [33].

Microstructural observations were performed on the surface of samples, using a Field Emission Scanning Electron Microscope (FESEM, Carl Zeiss Merlin) fitted with an energy dispersive spectrometry (EDS) analyzer. Several micrographs of the samples have been used to analyze the different phases and their distribution. Oxygen content has been determined by cerimetric titration

following the procedure described in previous works [34]. Electrical resistivity and Seebeck coefficient were simultaneously determined by the standard dc four-probe technique in a LSR-3 measurement system (Linseis GmbH), in the steady state mode and at temperatures ranging from 50 to 800 ºC under He atmosphere. From the resistivity values, the activation energy and the relative carrier concentration for each sample have been estimated. Moreover, with the electrical resistivity and thermopower data, the power factor has been calculated in order to determine the samples performances. These properties have been compared with the results obtained in the undoped samples and with those reported in the literature at low temperatures (~ 50 ºC), where oxygen diffusion is negligible, to avoid the influence of the atmosphere on the compared values.

3. Results and discussion

Powder XRD patterns for the different $Ca_{3-x}Sr_xCo_4O_9$ samples are displayed in Fig. 1 (from 5 to 40º for clarity). From these data, it is clear that all the samples have very similar diffraction patterns. In these plots, the peak marked by # belongs to the (111) diffraction plane of Si, used as reference. In Fig. 1a, corresponding to the undoped samples, major peaks are associated to the thermoelectric $Ca_3Co_4O_9$ phase, indicated by its reflection planes, in agreement with previously reported data [35]. When Sr is added to the samples, some new peaks appear (shown by * in Fig 1e), indicating the $Ca_3Co_2O_6$ phase formation [35]. On the other hand, careful observation of these diagrams shows that there is no Sr-containing secondary phase which is a clear indication that Sr has entered into the $Ca_3Co_4O_9$ and/or $Ca_3Co_2O_6$ phases. This Sr incorporation into

the $Ca_3Co_4O_9$ structure has no noticeable effect on the angles at which the cobaltite peaks appear due to the very small amounts of Sr.

Fig. 2 shows SEM micrographs performed on the surface of some representative samples. In the figure, it can be clearly seen that all samples are composed by randomly oriented plate-like grains with similar sizes. When observing the samples in more detail, it has been found that major phase is the thermoelectric $Ca_3Co_4O_9$ one (grey contrast, #1) which can be observed as well defined plate-like grains. $Ca_3Co_2O_6$ secondary phase (#2) can be also seen in all samples as a slightly darker grey contrast. In the case of undoped samples, the amount of secondary phase is small enough to avoid its identification by powder XRD. As a consequence, all these observations are in good agreement with the above discussed XRD data. On the other hand, EDS analysis has shown that Sr incorporation is produced in both crystal structures, the $Ca_3Co_4O_9$ and $Ca_3Co_2O_6$ phases. Moreover, Sr is preferentially incorporated in the first one, which shows a Sr-substitution slightly higher than the theoretical additions while for the second one, the amount of Sr is reduced to about a half of the theoretical additions. The fact that Sr content in the $Ca_3Co_2O_6$ phase is lower than the amount in the $Ca_3Co_4O_9$ one can be associated to its smaller rock salt layer c-parameter.

Other interesting feature which can be observed in Fig. 2, is that the samples are not fully dense and some porosity can be observed in the micrographs. This is due to the relatively low temperature stability of the thermoelectric phase (maximum stability temperature ~ 926 ºC), compared with the minimum temperature to produce a liquid phase (~ 1350 ºC) [35]. The great difference between both temperatures leads to a very slow densification process at the

sintering temperatures (~ 910 ºC), explaining the porosity obtained in these samples.

In order to evaluate the samples density, apparent density measurements have been performed on at least 4 samples for each composition. They were measured and weighed for three times to minimize the errors. The calculated apparent densities, together with their standard error, are represented in Fig. 3 *vs.* Sr contents. In the figure, it is clear that samples density increases around 5% from the undoped sample to the 0.05 Sr-doped one, and decreasing for further doping. These differences on the apparent density imply that they are ranging between ~ 75% of the theoretical one for the undoped samples and ~ 79% for the 0.05 Sr-doped one. Anyway, these variations are small enough to assume that density values practically have no effect on the electrical behaviour of the samples.

Fig. 4 shows the variation of the Seebeck coefficient with the temperature, as a function of the Sr doping. In the plot, it can be clearly seen that the sign of the thermopower is positive for the entire measured temperature range, which confirms a conduction mechanism mainly governed by holes. The values of the Seebeck coefficient increase with temperature, with similar behaviour for all the samples. The main differences between samples are observed at high temperatures, as the room temperature values are approximately the same for all samples, independently of Sr content. This measured value (around 135 μV/K) is slightly higher than those reported elsewhere for Sr-doped samples (~ 130 μV/K) at the same temperature [36]. The maximum measured Seebeck coefficient value (~ 220 μV/K) at 800 ºC corresponds to the 0.07 Sr-doped samples, around 10 % higher than the obtained for the undoped ones.

Moreover, S values at 625 ºC (~ 195 μV/K) are also higher than the best values obtained for undoped $Ca_3Co_4O_9$ samples sintered and textured by spark plasma sintering (170-175 μV/K) at the same temperature [37]. The relatively similar values obtained for the undoped and the Sr-doped samples indicate that Sr doping does not affect, in a great extent, the $Ca_3Co_4O_9$ conduction band [38].

The temperature dependence of electrical resistivity, as a function of the Sr content, is shown in Fig. 5. As can be clearly seen, the ρ (T) curves show a decrease of the measured resistivity from 0.00 to 0.07 Sr substitution. Higher Sr contents slightly increases resistivity, compared with the 0.07 Sr-doped samples. These curves reflect a slope change at about 400 ºC, from semiconducting-like ($d\rho/dT \leq 0$) to metallic-like ($d\rho/dT \geq 0$) one. The decrease of room temperature resistivity values with increasing Sr content is in agreement with previous works which demonstrate that the raise in the rock-salt layer dimensions produce a decrease of resistivity [7,26,39]. In any case, the lowest measured room temperature resistivity values (~ 15 mΩ.cm for the 0.07 and 0.10 Sr-substituted samples) is around the best values obtained for $Ca_3Co_4O_9$ samples sintered and textured by spark plasma sintering (15-18 mΩ.cm) [37] and about 25 % lower than the undoped samples prepared in this work.

In order to explain the resistivity behaviour of these samples, it should be considered that the temperature dependence of the electrical conductivity, in the semiconductor behaviour zone, can be described as:

$$\sigma.T \propto \exp(-E/k_B.T)$$

where E, k_B, and T are the activation energy, Boltzmann constant, and absolute temperature, respectively. The activation energy values are obtained from the log (σT) *versus* 1/T plot as the curve fit slope in the different samples below T*,

as illustrated in Fig. 6. T* is defined as the temperature where the behaviour of the samples changes from semiconducting-like to metallic-like one. The calculated values have been found to be around 40 meV in all cases, confirming that Sr addition does not modify appreciably the $Ca_3Co_4O_9$ conduction band. On the other hand, two differences between doped and undoped samples can be pointed out from this graph. Firstly, Sr addition shift the T^* to lower temperature values, indicating a change to metallic-like behaviour at lower temperature due to the fact that Sr doping increases the metallic characteristics of the compound. Secondly, the carrier concentration is increased when Sr is added to the samples, as the log (σT) *versus* 1000/T curves appear at higher values. Under the assumption that these changes in conductivity are mainly due to variations on the hole concentration, an increase between 30 and 40 % is produced when Sr is added between 0.01 and 0.07, respectively. These points clearly agree with the determined electrical resistivity values.

In order to evaluate the thermoelectric performances of these materials, the power factor has been calculated. The temperature dependence of the power factor, calculated from the data represented in Figs. 4 and 5, is plotted in Fig. 7. When considering PF values at around 50 ºC (~ room temperature), it can be clearly seen that all the Sr-doped samples possess higher PF values than the undoped ones. The maximum increase is obtained for the 0.07 Sr-doped samples (~ 33 % higher than the undoped ones). The highest PF value obtained at 800 ºC (around 0.30 $mW/K^2.m$) for the 0.07 Sr-doped samples is about 15 % higher than the highest values reported for Sr-doped samples prepared using the conventional solid state method (~ 0.26 $mW/K^2.m$) [36] and

relatively close to the values obtained in samples sintered and textured by spark plasma sintering (~ 0.32 mW/K^2.m) [37].

4. Conclusions

This paper demonstrates that Sr can substitute Ca in $Ca_{3-x}Sr_xCo_4O_9$ in small proportions ($x \leq 0.07$) without appreciably modifying the crystal structure and improving the thermoelectric properties. Further Sr addition slightly diminishes thermoelectric performances. The optimal Sr for Ca substitution has been determined using the values of the power factor at 50 and 800 ºC, which is maximum for the 0.07 Sr-doped samples with values around 0.12 and 0.30 mW/K^2.m, respectively, which are about 30 and 50 % higher than the obtained for the undoped samples at these temperatures. Moreover, the value at 800 ºC is also higher than the highest one obtained in Sr-doped samples prepared by the classical solid state method and very close to the obtained in textured samples produced by spark plasma sintering under pressure.

Acknowledgements

The authors wish to thank the Gobierno de Aragón (Research Groups T12 and T87) for financial support. The technical contributions of C. Estepa, and C. Gallego are also acknowledged. Sh. Rasekh also acknowledges a JAE-PreDoc 2010 grant from CSIC.

References

[1] D.M. Rowe, in: D.M. Rowe (Ed.), Thermoelectrics Handbook: Macro to Nano, 1st edn, CRC Press, Boca Raton, FL, 2006, pp. 1-3–1-7.

[2] G. Mahan, B. Sales, J. Sharp, Thermoelectric materials: New approaches to an old problem, Phys. Today 50 (1997) 42-47.

[3] H. Naito, Y. Kohsaka, D. Cooke, H. Arashi, Development of a solar receiver for a high-efficicency thermionic/thermoelectric conversion system, Solar Energy 58 (1996) 191-195.

[4] C. M. Kim, Y. J. Hwang, Y. H. Ryu, Air conditioner for individual cooling/heating, US Patent US6393842. May, 2002.

[5] I. Terasaki, Y. Sasago, K. Uchinokura, Large thermoelectric power in $NaCo_2O_4$ single crystals, Phys. Rev. B 56 (1997) 12685-12687.

[6] M. A. Madre, Sh. Rasekh, J. C. Diez, A. Sotelo, New solution method to produce high performance thermoelectric ceramics: A case study of Bi-Sr-Co-O, Mater. Lett. 64 (2010) 2566-2568.

[7] A. Sotelo, Sh. Rasekh, M. A. Madre, E. Guilmeau, S. Marinel, J. C. Diez, Solution-based synthesis routes to thermoelectric $Bi_2Ca_2Co_{1.7}O_x$, J. Eur. Ceram. Soc. 31 (2011) 1763-1769.

[8] G. Constantinescu, Sh. Rasekh, M. A. Torres, M. A. Madre, J. C. Diez, A. Sotelo, Enhancement of the high-temperature thermoelectric performance of $Bi_2Ba_2Co_2O_x$ ceramics, Scripta Mater. 68 (2013) 75-78.

[9] R. Funahashi, I. Matsubara, H. Ikuta, T. Takeuchi, U. Mizutani, S. Sodeoka, An oxide single crystal with high thermoelectric performance in air, Jpn. J. Appl. Phys. 39 (2000) L1127-1129.

[10] A. Sotelo, G. Constantinescu, Sh. Rasekh, M. A. Torres, J. C. Diez, M. A. Madre, Improvement of thermoelectric properties of $Ca_3Co_4O_9$ using soft chemistry synthetic methods, J. Eur. Ceram. Soc. 32 (2012) 2415-2422.

[11] A. Maignan, S. Hébert, M. Hervieu, C. Michel, D. Pelloquin, D. Khomskii, Magnetoresistance and magnetothermopower properties of Bi/Ca/Co/O and Bi(Pb)/Ca/Co/O misfit layer cobaltites, J. Phys.: Condens. Matter. 15 (2003) 2711-2723.

[12] H. Itahara, C. Xia, J. Sugiyama, T. Tani, Fabrication of textured thermoelectric layered cobaltites with various rock salt-type layers by using β-$Co(OH)_2$ platelets as reactive templates, J. Mater. Chem. 14 (2004) 61-66.

[13] A. Maignan, D. Pelloquin, S. Hébert, Y. Klein, M. Hervieu, Thermoelectric power in misfit cobaltites ceramics: Optimization by chemical substitutions, Bol. Soc. Esp. Ceram. V. 45 (2006) 122-125.

[14] S. Demirel, M. A. Aksan, S. Altin, Low temperature electrical and thermal transport properties of the $Ca_{3-x}Sb_xCo_4O_9$ system, J. Mater. Sci.: Mater. Electron. 23 (2012) 2251-2256.

[15] A. Sotelo, Sh. Rasekh, E. Guilmeau, M. A. Madre, M. A. Torres, S. Marinel, J. C. Diez, Improved thermoelectric properties in directionally grown $Bi_2Sr_2Co_{1.8}O_y$ ceramics by Pb for Bi substitution, Mater. Res. Bull. 46 (2011) 2537-2542.

[16] A. Sotelo, E. Guilmeau, Sh. Rasekh, M. A. Madre, S. Marinel, J. C. Diez, Enhancement of the thermoelectric properties of directionally grown Bi-Ca-Co-O through Pb for Bi substitution, J. Eur. Ceram. Soc. 30 (2010) 1815-1820.

[17] Sh. Rasekh, M. A. Madre, J. C. Diez, E. Guilmeau, S. Marinel, A. Sotelo, Effect of Pb substitution on the thermoelectrical properties of textured

$Bi_2Ca_2Co_{1.7}O_y$ ceramics prepared by a polymer solution method, Bol. Soc. Esp. Ceram. V. 49 (2010) 371-376.

[18] A. Sotelo, M. A. Torres, G. Constantinescu, Sh. Rasekh, J. C. Diez, M. A. Madre, Effect of Ag addition on the mechanical and thermoelectric performances of annealed $Bi_2Sr_2Co_{1.8}O_x$ textured ceramics, J. Eur. Ceram. Soc. 32 (2012) 3745-3751.

[19] A. Sotelo, Sh. Rasekh, G. Constantinescu, M. A. Torres, M. A. Madre, J. C. Diez, Improvement of textured $Bi_{1.6}Pb_{0.4}Sr_2Co_{1.8}O_x$ thermoelectric performances by metallic Ag additions, Ceram. Int. 39 (2013) 1597-1602.

[20] V. Garnier, R. Caillard, A. Sotelo, G. Desgardin, Relationship among synthesis, microstructure and properties in sinter-forged Bi-2212 ceramics, Physica C 319 (1999) 197-208.

[21] D. Kenfaui, D. Chateigner, M. Gomina, J. G. Noudem, Anisotropy of the mechanical and thermoelectric properties of hot-pressed single-layer and multilayer thick $Ca_3Co_4O_9$ ceramics, Int. J. Appl. Ceram. Technol. 8 (2011) 214-226.

[22] J. G. Noudem, D. Kenfaui, D. Chateigner, M. Gomina, Granular and lamellar thermoelectric oxides consolidated by spark plasma sintering, J. Electron. Mater. 40 (2011) 1100-1106.

[23] Y. Liu, Y. Lin, C.-W. Nan, Z. Shen, Preparation of $Ca_3Co_4O_9$ and improvement of its thermoelectric properties by spark plasma sintering, J. Am. Ceram. Soc. 88 (2005) 1337-1340.

[24] S. Marinel, D. Bourgault, O. Belmont, A. Sotelo, G. Desgardin, Microstructure and transport properties of YBCO zone melted samples

processed in a microwave cavity and infra-red furnace, Physica C 315 (1999) 205-214

[25] A. Sotelo, E. Guilmeau, M. A. Madre, S. Marinel, J. C. Diez, M. Prevel, Fabrication and properties of textured Bi-based cobaltite thermoelectric rods by zone melting, J. Eur. Ceram. Soc. 27 (2007) 3697-3700.

[26] J. C. Diez, Sh. Rasekh, M. A. Madre, E. Guilmeau, S. Marinel, A. Sotelo, Improved thermoelectric properties of Bi-M-Co-O (M = Sr, Ca) misfit compounds by laser directional solidification, J. Electron. Mater. 39 (2010) 1601-1605.

[27] N. M. Ferreira, Sh. Rasekh, A. J. S. Fernandes, F. M. Costa, M. A. Madre, J. C. Diez, A. Sotelo, Electrical polarization effect on $Bi_2Ca_2Co_{1.7}O_x$ thermoelectrics grown by laser floating zone, Microsc. Microanal. 18 (2012) 93-94.

[28] N. M. Ferreira, Sh. Rasekh, F. M. Costa, M. A. Madre, A. Sotelo, J. C. Diez, M. A. Torres, New method to improve the grain alignment and performance of thermoelectric ceramics, Mater. Lett. 83 (2012) 144-147.

[29] M. M. Seabaugh, I. H. Kerscht, C. L. Messing, Texture development by templated grain growth in liquid-phase-sintered alpha-alumina, J. Am. Ceram. Soc. 80 (1997) 1181-1188.

[30] A. Sotelo, E. Guilmeau, M. A. Madre, S. Marinel, S. Lemmonier, J. C. Diez, $Bi_2Ca_2Co_{1.7}O_x$ thermoelectric ceramics textured by laser floating zone method, Bol. Soc. Esp. Ceram. V. 47 (2008) 225-228.

[31] J. C. Diez, E. Guilmeau, M. A. Madre, S. Marinel, S. Lemmonier, A. Sotelo, Improvement of $Bi_2Sr_2Co_{1.8}O_x$ thermoelectric properties by laser floating zone texturing, Solid State Ionics 180 (2009) 827-830.

[32] Sh. Rasekh, G. Constantinescu, M. A. Torres, M. A. Madre, J. C. Diez, A. Sotelo, Growth rate effect on microstructure and thermoelectric properties of melt grown $Bi_2Ba_2Co_2O_x$ textured ceramics, Adv. Appl. Ceram. 111 (2012) 490-494.

[33] Y. C. Liou, W. C. Tsai, W. Y. Lin, U. R. Lee, Synthesis of $Ca_3Co_4O_9$ and $CuAlO_2$ ceramics of the thermoelectric application using a reaction-sintering process, J. Aust. Ceram. Soc. 44 (2008) 17–22.

[34] M. A. Madre, F. M. Costa, N. M. Ferreira, A. Sotelo, M. A. Torres, G. Constantinescu, Sh. Rasekh, J. C. Diez, Preparation of high-performance $Ca_3Co_4O_9$ thermoelectric ceramics produced by a new two-step method, J. Eur. Ceram. Soc. 33 (2013) 1747-1754.

[35] E. Woermann, A. Muan, Phase equilibria in the system CaO-cobalt oxide in air, J. Inorg. Nucl. Chem. 32 (1970) 1455-1459.

[36] O-J. Kwon, W. Jo, S. Yoon, D. Shin, H. You, K. Choi, J.-S. Kim, C. Park, Relation between Seebeck coefficient and lattice parameters of $(Ca_{2-y}Sr_yCoO_3)_xCoO_2$, J. Electron. Mater. 41 (2012) 1513-1518.

[37] D. Kenfaui, G. Bonnefont, D. Chateigner, G. Fantozzi, M. Gomina, J. G. Noudem, $Ca_3Co_4O_9$ ceramics consolidated by SPS process: Optimisation of mechanical and thermoelectric properties, Mater. Res. Bull. 45 (2010) 1240-1249.

[38] J. C. Diez, M. A. Torres, Sh. Rasekh, G. Constantinescu, M. A. Madre, A. Sotelo, Enhancement of $Ca_3Co_4O_9$ thermoelectric properties by Cr for Co substitution, Ceram. Int. 39 (2013) 6051-6056.

[39] M. A. Torres, A. Sotelo, Sh. Rasekh, I. Serrano, G. Constantinescu, M. A. Madre, J. C. Diez, Improvement of thermoelectric properties of $Bi_2Sr_2Co_{1.8}O_x$ through solution synthetic methods, Bol. Soc. Esp. Ceram. V. 51 (2012) 1-6.

Figure captions:

Figure 1. Powder X-ray diffraction patterns obtained for the $Ca_{3-x}Sr_xCo_4O_9$ samples; x = 0.00 (a); 0.01 (b); 0.03 (c); 0.05 (d); 0.07 (e); and 0.10 (f). The diffraction planes indicate the $Ca_3Co_4O_9$ phase, those indicated by a * the $Ca_3Co_2O_6$ one. The # symbol denotes the (111) plane of Si used as internal reference.

Figure 2. Surface SEM micrographs of $Ca_{3-x}Sr_xCo_4O_9$ samples for x = 0.00 (a); 0.01 (b); 0.07 (c); and 0.10 (d) showing the randomly oriented plate-like grains. The two different contrasts have been associated to: 1) $Ca_3Co_4O_9$; and 2) $Ca_3Co_2O_6$ phases.

Figure 3. Apparent density values, together with their standard error, as a function of the Sr addition.

Figure 4. Temperature dependence of the Seebeck coefficient as a function of Sr content in $Ca_{3-x}Sr_xCo_4O_9$ samples, for x = 0.00 (●); 0.01 (▼); 0.03 (■); 0.05 (◆); 0.07 (▲); and 0.10 (◣).

Figure 5. Temperature dependence of the electrical resistivity, as a function of Sr content in $Ca_{3-x}Sr_xCo_4O_9$ samples, for x = 0.00 (●); 0.01 (▼); 0.03 (■); 0.05 (◆); 0.07 (▲); and 0.10 (◣).

Figure 6. Log (σT) *versus* 1000/T plot for all the $Ca_{3-x}Sr_xCo_4O_9$ samples, for x = 0.00 (●); 0.01 (▼); 0.03 (■); 0.05 (◆); 0.07 (▲); and 0.10 (◣). The slopes of the fittings are nearly the same in all cases, below T*. T* indicates the metallic-to-semiconducting transition temperature.

Figure 7. Temperature dependence of the power factor as a function of Sr content in $Ca_{3-x}Sr_xCo_4O_9$ samples, for x = 0.00 (●); 0.01 (▼); 0.03 (■); 0.05 (◆); 0.07 (▲); and 0.10 (◣).

Figure 1

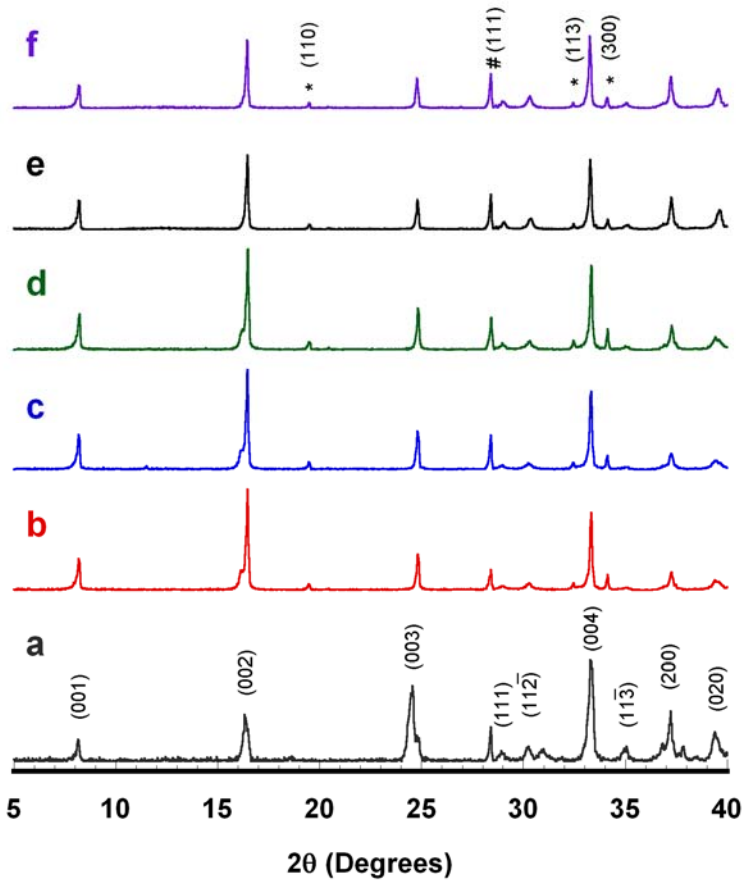
f
e
d
c
b
a
(110)
*
(111)
(113)
*
(300)
*
(001)
(002)
(003)
(111)
(11$\bar{2}$)
(004)
(11$\bar{3}$)
(200)
(020)
5
10
15
20
25
30
35
40
2θ (Degrees)

Figure 2

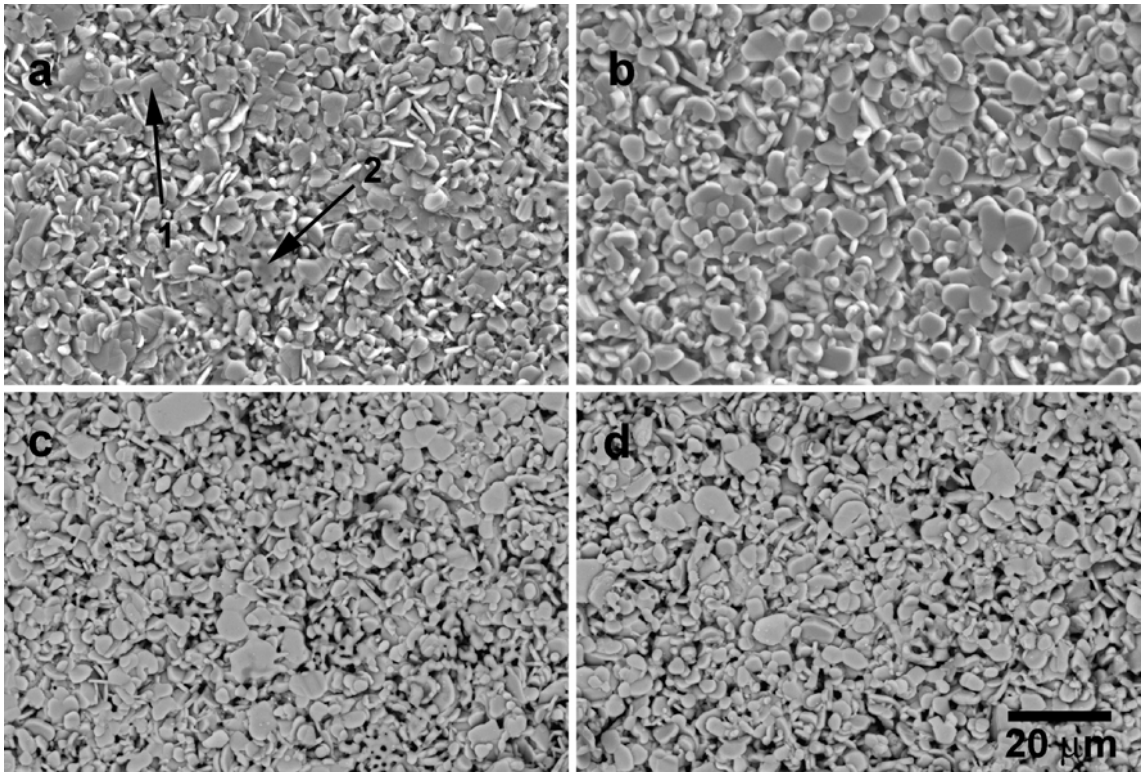

Figure 3

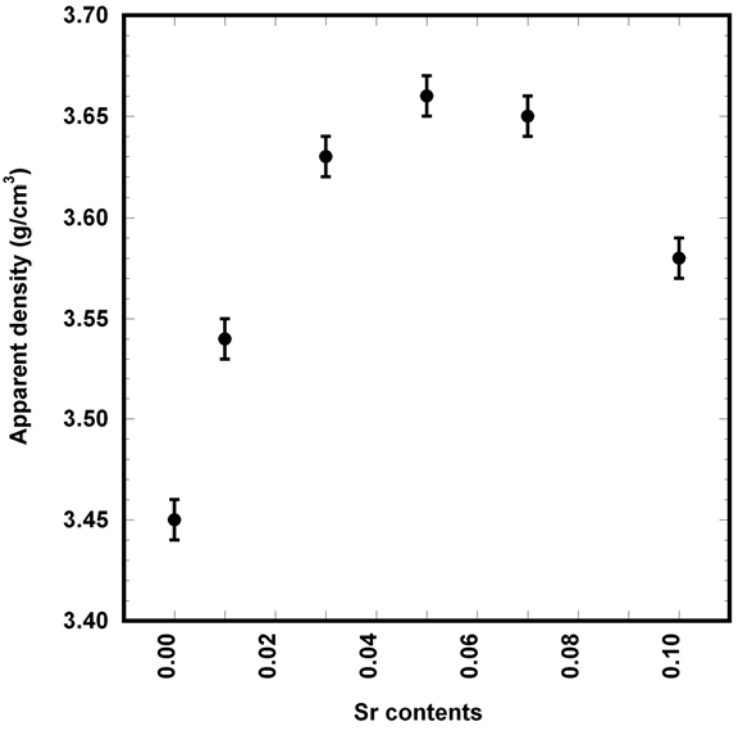
3.70
3.65
3.60
3.55
3.50
3.45
3.40
Apparent density (g/cm3)
0.00
0.02
0.04
0.06
0.08
0.10
Sr contents

Figure 4

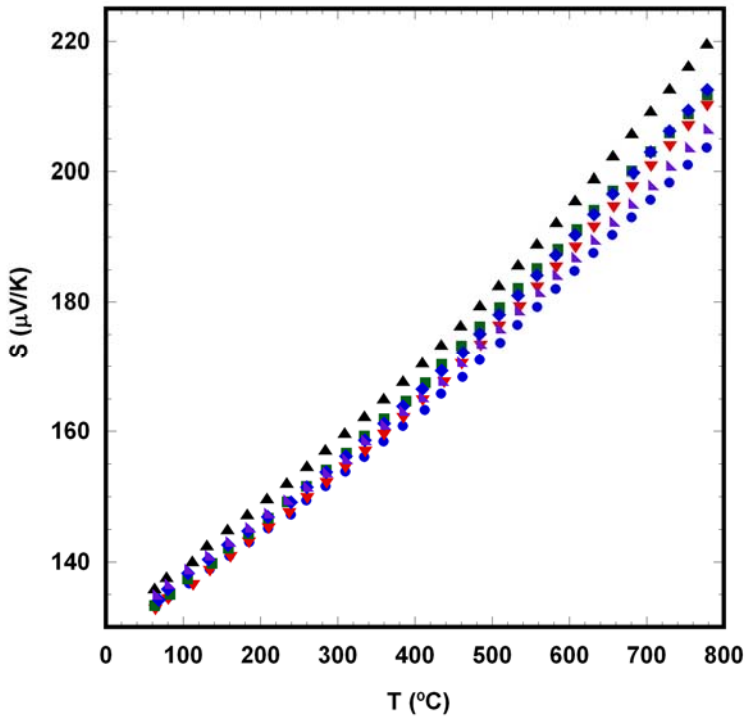

Figure 5

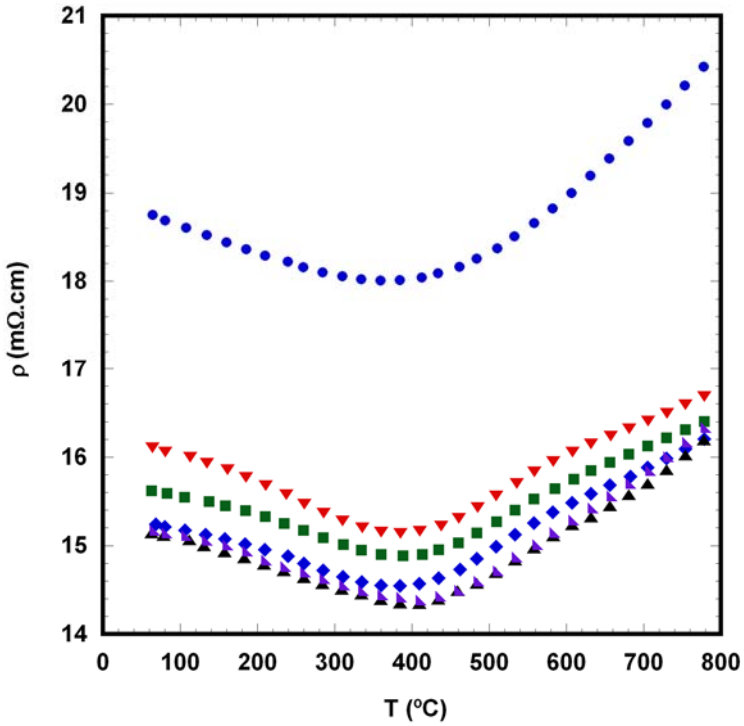

Figure 6

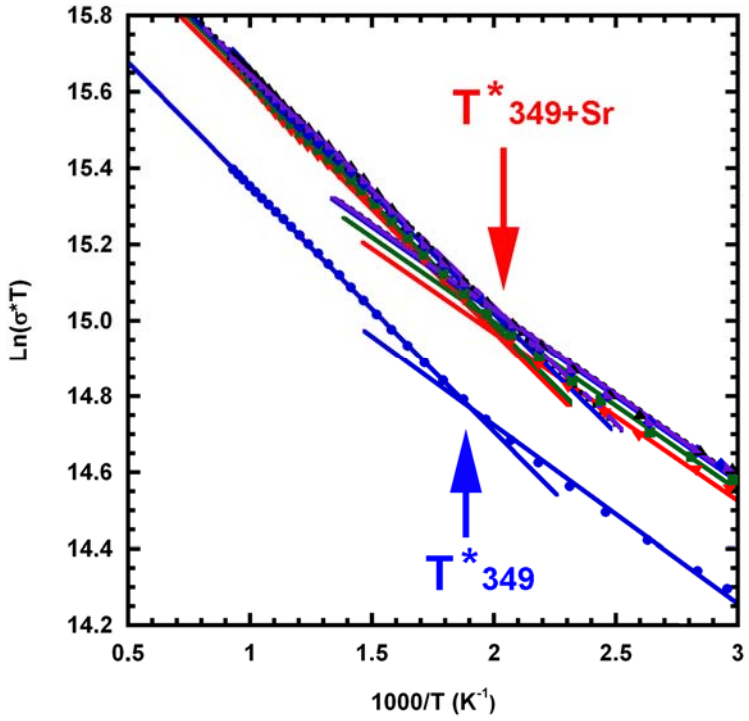
15.8
15.6
15.4
15.2
15.0
14.8
14.6
14.4
14.2
Ln(σ*T)
0.5
1
1.5
2
2.5
3
1000/T (K-1)
T*349+Sr
T*349

Figure 7

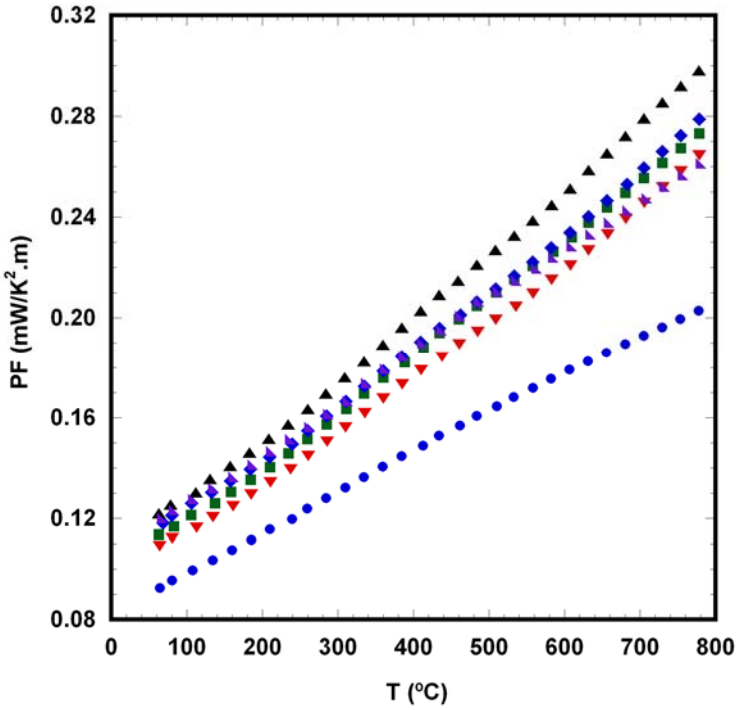
0.32
0.28
0.24
0.20
0.16
0.12
0.08
PF (mW/K^2.m)
0
100
200
300
400
500
600
700
800
T (ºC)